Chapter 2
Electrical Impedance Spectroscopy

Pedro Bertemes-Filho

2.1 Electrical Impedance Spectroscopy Basics

The world we live in is surrounded by electromagnetic waves. When electromagnetic (EM) waves interact with matter, radiation may be transmitted (e.g. visible light is transmitted by water), scattered (e.g. small particles suspended in water scatter blue light preferentially) and absorbed (e.g. the red part of visible light is absorbed by copper sulphate solution which causes the remaining transmitted light to appear blue) (Hollas 1998).

The absorption of electromagnetic (EM) radiation can involve many processes, but they all depend upon frequency and hence energy. For example, very high frequency radiation is ionising. The spectrum of the nonionising EM waves is considered to be below the infrared waves, i.e. less than 3 THz. The equation $E = h\nu$ gives the relationship between the energy E of the radiation and the frequency ν, where $h = 6.626 \times 10^{-34}$ Js is the Planck's constant (Brown et al. 1999). Figure 2.1 shows some of the major components of the EM spectrum and the associated energies and frequencies. The energies are expressed in terms of electronvolt, i.e. $1\ \text{eV} = 1.6022 \times 10^{-22}$ kJ.

Any study of how absorption depends upon frequency may be considered as *spectroscopy*. They are in the range 100 Hz—10 MHz where absorption is mainly determined by the cellular structure of tissue. Thus we may define *electrical impedance spectroscopy* (EIS) as the study of the interaction of an alternating electrical field with biological tissue in the frequency range 100 Hz–10 MHz (see Fig. 2.1).

P. Bertemes-Filho (✉)
Departamento de Engenharia Elétrica, Universidade do Estado de Santa Catarina, Joinville, Santa Catarina, Brazil
e-mail: pedro.bertemes@udesc.br

F. Simini, P. Bertemes-Filho (eds.), *Bioimpedance in Biomedical Applications and Research*, https://doi.org/10.1007/978-3-319-74388-2_2

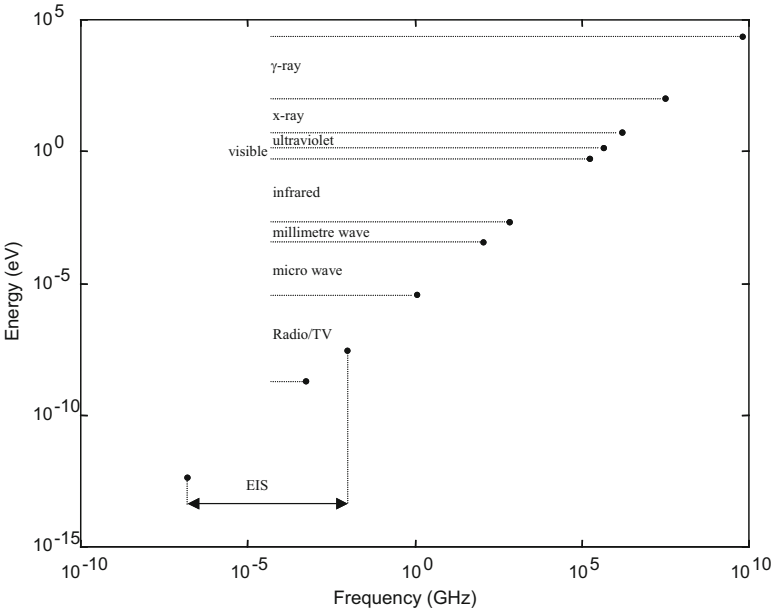

Fig. 2.1 Regions of the electromagnetic spectrum

EIS technique is related to the absorption phenomena of the EM waves, which is measured by varying the frequency of the applied "radiation" (e.g. electrical field) and plotting the "energy absorbed" (e.g. potential induced) by the sample at each frequency. The resultant plotting is called a *spectrum* which may contain the intensity of the absorption, i.e. electrical impedance.

The general approach in EIS is to apply an electrical stimulus (a known voltage or current) to the material and then to observe the resulting current or voltage. The stimulus can be applied in many forms. McAdams (1987) gives three mainly possible forms, as described in the following:

1. *Step function*: a step voltage $v(t)$ is applied at $t = 0$ to the material and a time-varying current $i(t)$ is measured. It is then Fourier-transformed into the frequency domain in order to calculate the frequency-dependent impedance.
2. *Noise signal*: a continuous voltage composed of random noise with energy over a known frequency range is applied to the material, and the resulting current is measured and then Fourier-transformed into the frequency domain.
3. *Sinusoidal signal*: a single-frequency voltage or current is applied to the material, and the resulting frequency-dependent current or voltage is measured. The response is measured in the frequency range of interest in terms of phase shift and amplitude or real and imaginary parts.

Other types of stimulus have been recently used in EIS (Min et al. 2007), such as chirp signal (Nahvi and Hoyle 2009) and binary multifrequency signals (Land et al.

2011; Yang et al. 2010). The first is based on short frequency-swept signals, whose advantage is that the characteristics of a biological object can be obtained in a wide frequency range during a very short measurement cycle (Paavle et al. 2012). The second is based on the excitation of waveforms with spectrally sparse distribution of frequency components, which is basically a technique for improving the Signal to Noise Ratio (SNR) of bioimpedance measurements.

Most EIS use current injection technique for stimulating the material under study, and then the resulting voltage is measured (Bertemes-Filho 2002). However, voltage stimulus may also be used and then the resulting current is measured instead. The current technique is a load-independent circuit, whereas the voltage one is more stable and easy to generate. It has been shown that non-linearities can arise in the electrodes used both to inject current and measure voltage (Pliquett et al. 2010). This effect is particularly important when using small electrodes with high impedance. Nevertheless, electrode-tissue interface issues have been investigated since Oliver Heaviside introduced the concept of electrical impedance in the 1880s.

EIS technique involves measuring electrical impedance Z, admittance Y, the impedance modulus $|Z|$, or the permittivity ε as a function of frequency in order to characterise the biological material under study. Cole and Cole (1941) showed that many tissues exhibit charges of complex permittivity ε^* which can be described by a relatively simple equation. This is considered later in this chapter.

EIS can be assisted by the use of electrical equivalent circuits to represent biological tissue, which is mostly studied over the last decades. Such equivalent circuits can be used to describe parameters which characterise a particular impedance spectrum. However, the representation of tissue is not easy as it must involve complex combination of resistors and capacitors to represent the conductivity and insulating components of tissue (Paterno et al. 2012). Some equivalent circuit models will be described in this chapter.

2.2 Tissue Impedance Basics

Tissues exhibit the properties of both conductors and dielectrics, i.e. they contain both free and bound (fixed) charges. As a result tissue impedance contains both conduction and dielectric terms. The conductivity term (σ) appears to account for the movement of free charges, and the relative permittivity term (ε_r) appears to account for movement of bound charges in the dielectric due to an applied electrical field of unit amplitude.

At the frequencies tissue can be considered as a collection of membranes separating intracellular and extracellular spaces. We can describe the electrical properties of tissue by considering that the current flows in the extracellular and in the intracellular fluids of tissue at low frequency and high frequency, respectively. The presence of current flow inside the cell is likely due to the cell membrane constituents. Cell membranes are composed mainly of proteins and water-insoluble lipids. Hence the membranes are highly resistive (conductivity less than 10^{-7} S/m)

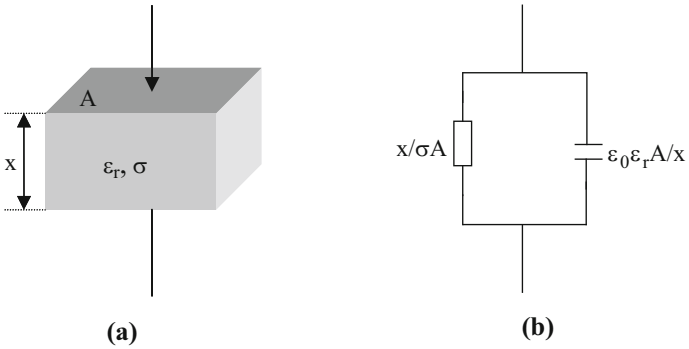

Fig. 2.2 (**a**) Idealised slab of tissue, where A is the area, x is the thickness, ε_r is the relative permittivity and σ is the conductivity. (**b**) Equivalent circuit of the slab of tissue represented by a resistance in parallel with a capacitance, where ε_0 is the permittivity of free space (8.85×10^{-12} F/m)

and mainly capacitive (typically 10^{-2} F/m^2) (Pethig 1984). Therefore, it is expected that impedance will drop with increasing frequency. Measurements have shown that intracellular resistivity is typically higher than 0.6 Ωm, whereas extracellular resistivity is within the range 0.5–0.6 Ωm (González-Correa et al. 1999).

A slab of tissue of area A and thickness x may have conductivity σ and relative permittivity ε_r, as shown in Fig. 2.2a. We can represent this tissue by a model consisting of a resistance in parallel with a capacitance, as shown in Fig. 2.2b. However, this model cannot explain the whole of tissue properties over a wide range of frequencies. The electrical properties may not be homogeneous within the slab and both σ and ε_r may be function of frequency.

Both relative permittivity ε_r and conductivity σ are found to be a function of frequency. The permittivity of a real dielectric, which is represented as a slab of tissue in figure, can be related to an admittance Y^*, where the symbol * represents a complex variable. Mathematically, the admittance Y^* can be considered either in terms of a complex conductivity σ^* (see Eq. 2.1) or in terms of a complex permittivity ε^* which is defined by a complex capacitance C^* (see Eq. 2.2).

$$Y^* = G + j\omega C = \frac{A}{x} \cdot (\sigma + j\omega\varepsilon_0\varepsilon_r) = \frac{A}{x} \cdot \sigma^* \tag{2.1}$$

$$C^* = \frac{Y^*}{j\omega} = \frac{A}{x} \cdot \left(-\frac{j\sigma}{\omega} + \varepsilon_0\varepsilon_r\right) = \frac{A}{x} \cdot \varepsilon_0\varepsilon^* \tag{2.2}$$

where ω is the angular frequency in radians and $j = (-1)^{1/2}$.

It can be noticed in Eq. (2.1) that as the frequency tends to zero, the conductivity becomes dominant, whereas permittivity is dominant at high frequencies (see Eq. 2.2).

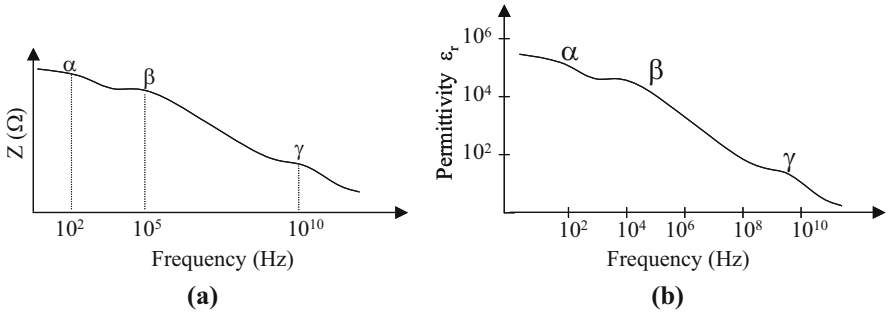

Fig. 2.3 (**a**) Theoretical impedance diagram showing the α, β and γ dispersions for muscle tissue; (**b**) an idealised plot of the relative permittivity as a function of frequency for a typical biological tissue (modified from Pethig 1987)

The frequency dependence of tissue is known as dispersion. Within the frequency range covered by this chapter, the cellular structure of tissue produces the dispersion. At higher frequencies, dispersion arises from the ability of molecules to reorient in an applied field. Dispersions also occur at lower frequencies but their origin is not clear. The dispersions within biological tissue are often separated into three regions: α (*alpha*), β (*beta*) and γ (*gamma*).

We would thus expect that the electrical impedance Z of biological materials would be frequency-dependent over a wide range of frequencies. For example, the major dispersions of the impedance for muscle tissue can be seen in Fig. 2.3a (Pethig 1987), which covers the range from 100 Hz to 20 GHz. The origin of the α dispersion is still not well understood. When collections of cells are considered, the α dispersion is important. The β dispersion results mainly from the capacitive charging of the cell membranes, and the γ dispersion results mainly from the dielectric relaxation of free water. Figure 2.3b shows an idealised representation of these dispersions according to the relative permittivity of most biological tissue against frequency. This shows that the effective capacitance of tissue falls with increasing frequency.

In practice, tissue is not totally homogeneous or isotropic. Many biological tissues are highly anisotropic; that is, the conductivity in different directions is not the same. Anisotropy can be represented by three principal conductivities in three mutually perpendicular directions as determined by the structure of the material. Foster and Schwan (1989) have concluded that muscle tissue exhibits an extreme anisotropy, mainly at *alpha* dispersion frequencies.

So far, we have seen that the electrical impedance of biological tissue decreases with increasing frequency and this dependence on frequency was due to the cell membrane, which behaves like a capacitor. By considering the extracellular and intracellular constituents of tissue, we can relate them to the electrical equivalent circuit, as shown in Fig. 2.4.

However, this cell model does not represent the behaviour of the membrane impedance over a wide frequency range. Debye produced a similar model by considering the impedance of a suspension of free dipoles. He produced Eq. 2.3 for the complex relative permittivity ε_r^* of the suspension.

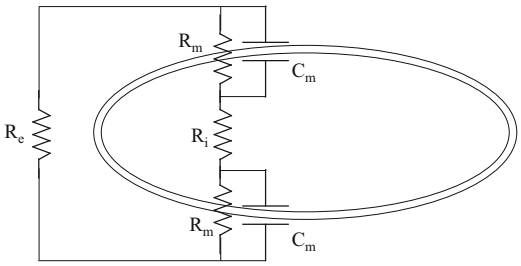

Fig. 2.4 Diagram schematic of the electrical cell model, where R_e is the extracellular fluid resistance, R_i is the intracellular fluid resistance, R_m is the membrane resistance and C_m is the membrane capacitance (redrawn from Webster 1990), which is here represented by the space between the ellipses

Fig. 2.5 Equivalent circuit for Eq. (2.3)

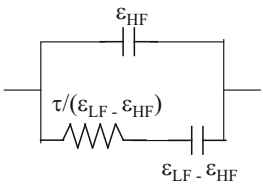

$$\varepsilon_r{}^* = \varepsilon_{\mathrm{HF}} + \frac{\varepsilon_{\mathrm{LF}} - \varepsilon_{\mathrm{HF}}}{1 + j\omega\tau} \tag{2.3}$$

where ε_r* is the complex relative permittivity, $\varepsilon_{\mathrm{HF}}$ is the permittivity at high frequency, $\varepsilon_{\mathrm{LF}}$ is the permittivity at low frequency and τ is the relaxation time constant. The equivalent circuit representation of this equation is shown in Fig. 2.5.

However, neither the Debye model nor the cell model can predict values for the relative permittivity over a wide frequency range. Cole and Cole (1941) took into account dispersion by including a dimensionless distribution parameter α in Eq. (2.3). α can be chosen to produce a good fit between a measured spectrum and Equation 2.4. It should be pointed out that the Cole Equation (2.4) is not derived from a model but was an empirical modification to the Debye equation:

$$\varepsilon_r{}^* = \varepsilon_{\mathrm{HF}} + \frac{\varepsilon_{\mathrm{LF}} - \varepsilon_{\mathrm{HF}}}{1 + (j\omega\tau)^{1-\alpha}} \tag{2.4}$$

where α is the dimensionless numerical constant to fit the data, which is not related to the *alpha* dispersion.

When $\alpha = 0$, Eqs. (2.3) and (2.4) are identical. The full analytic formulation for real and imaginary parts ($\varepsilon'$and ε'') of Eq. (2.4) can be seen in Cole and Cole (1941). As a result of Eq. (2.4), the membrane is a perfect capacitance (i.e. the membrane is fully ion impermeable) if α is equal to zero. On the other hand, the membrane is a pure resistance (i.e. the membrane is permeable for all ions) if α is equal to one.

2.3 Measuring Tissue Impedance

The ratio of the potential resulting between two electrodes in contact with tissue to the current injected between two other electrodes will be called "transfer impedance". All methods for measuring tissue transfer impedance use electrodes, which inject a known current into the tissue. The effect of electrodes on the measuring technique will be briefly described in this section.

Most tissue impedance spectroscopy systems involve the injection of a constant current into tissue at different frequencies and measuring the resultant voltages. The resultant voltage can be measured by using the same electrodes which were used for current injection (bipolar technique), or a separate pair of electrodes can be used for potential measurement (tetrapolar technique). Most tissue impedance measurements use the tetrapolar technique. However, both techniques will be described into this section. The accuracy of the measurements is dependent on the characteristics of the electronics. The key characteristics of these will also be described later in the chapter.

2.3.1 The Bipolar Technique

An impedance spectrum can be obtained by injecting current between two electrodes and measuring the resulting voltages between the same electrodes through which the current was injected. The impedance of skin and the electrode can be a problem for this kind of system due to unknown and varying contact impedance at each electrode site. Figure 2.6a shows the general concept of this system, where a voltage-controlled current source (VCCS) applies a constant current and a differential amplifier measures the voltage across the electrodes.

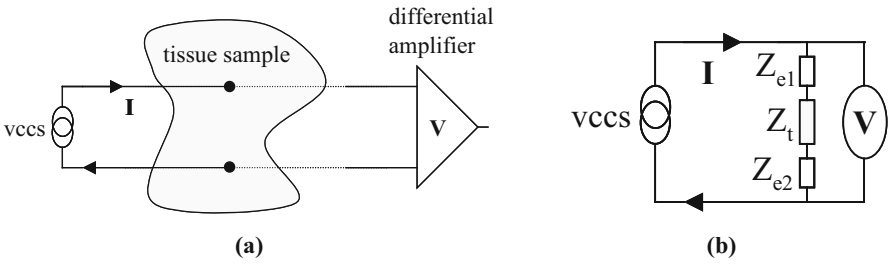

Fig. 2.6 (**a**) Bipolar constant current method to measure tissue impedance, where I is the drive current and V is the measured differential voltage; (**b**) equivalent circuit of two-electrode measurement, where Z_t is the tissue impedance and Z_{e1} and Z_{e2} are both the electrode impedances

It can be observed in Fig. 2.6b that there is only one possible measurement and there are three variables in the system (Z_{e1}, Z_{e2} and Z_t). Hence, the system is indeterminate. As a result, it is not possible to say if the change in the voltage V is due to tissue impedance Z_t changes or due to electrode impedance changes.

2.3.2 The Tetrapolar Technique

In the tetrapolar impedance method, a constant current is injected through one pair of electrodes, and the impedance-dependent voltage is measured with a second pair of electrodes. This technique was firstly introduced by Bouty in 1884. The method is relatively insensitive to changes in the electrode-subject impedance of both voltage-sensing and current-injecting electrodes (Raghed et al. 1992).

The insensitive conditions of the tetrapolar measurement are satisfied when the output impedance of the current generator Z_S and the input impedance of the differential amplifier Z_V are large as compared with the sum of the electrode and tissue impedances. In other words, the currents i_S and i_V can be assumed to be negligible. The tetrapolar measurement can be represented by an equivalent electrical circuit shown in Fig. 2.7.The equivalent circuit shown in Fig. 2.7 is a dual balance circuit (bipolar) for measuring the transfer impedance $T_Z = V/I$. By assuming equal electrode impedances, i.e. $Z_{e1} = Z_{e2} = Z_{e3} = Z_{e4} = Z$, the transfer impedance T_Z can be evaluated according to Eq. (2.5).

$$T_Z = \frac{Z_t}{1 + Z_t \cdot \left[\frac{4Z+Z_V+Z_S}{Z_V \cdot Z_S}\right] + 2Z \cdot \left[\frac{2Z+Z_V+Z_S}{Z_V \cdot Z_S}\right]} \tag{2.5}$$

In theory, the measured transfer impedance T_Z is assumed to be equal to the impedance Z_t measured across the tissue sample. However, it can be seen in

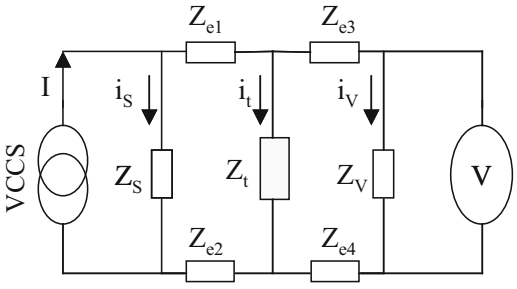

Fig. 2.7 Equivalent electrical circuit for the tetrapolar measurement, where I is the drive current, i_S is the equivalent leakage current because of the source impedance Z_S, i_t is the "real" current through the tissue, i_V is the current flowing through the input impedance Z_V of the differential amplifier and Z_{e1}, Z_{e2}, Z_{e3} and Z_{e4} are the electrode impedances

Eq. (2.5) that it will be the case only if Z_S and Z_V tend to infinity. In practice, stray capacitances connected to ground will decrease significantly Z_S and Z_V, especially at high frequencies. Hence, the non-idealised characteristics of the electronics will limit the measurements of tissue impedance.

2.3.3 Basic Hardware Concepts

Most transfer-impedance measurement systems use a constant multifrequency current for the driving system. Hence the most important characteristic in this system is the accuracy of the current generators, which should have a constant output current over a wide range of frequencies. Firstly, a voltage signal is generated in order to have it converted into a constant current. Most tissue impedance measurements use a sine wave or a pulse as the voltage signal in the drive system. The general characteristics of this will be described into this section.

As already shown here, there are mainly five types of methods to measure tissue impedance over a wide frequency range: (1) changing the frequency of the drive current and measuring the voltage (e.g. Griffiths and Ahmed 1987); (2) applying a current with a component containing multiple summed sine waves (e.g. Lozano et al. 1990); (3) applying a pulse, which contains a broad spectral energy, via current source (e.g. Record et al. 1992; Waterworth et al. 2000); (4) injecting either a current or voltage chirp signal (Nahvi and Hoyle 2009); and (5) applying current/voltage binary multifrequency signals (Land et al. 2011; Yang et al. 2010). The general principle of most EIS system for measuring the resulting voltage in order to calculate the transfer impedance is schematised in Fig. 2.8.

The sine wave is digitally generated and a VCCS circuit is used to convert it into a constant current. The voltage receive circuit measures the differential voltage between the electrodes. However, both circuits require a control circuit, for example, to select different electrode combinations from the probe and to set the voltage gain.

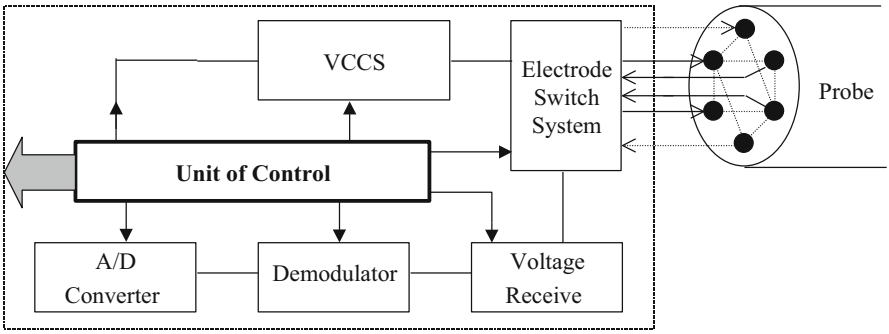

Fig. 2.8 General concepts of a system to measure transfer impedances by using a probe with six electrodes equally placed in a ring, where VCCS is the voltage-controlled current source

Other components required include a demodulator, low-pass filter and switches to measure the differential voltage from many different electrode combinations. Once the data are stored in memory, the measurements can be recovered and processed by computer, and then the transfer impedance can be calculated.

It is difficult to design a VCCS circuit to inject a constant current over a wide frequency range. The presence of parasitic capacitance to ground is a major factor which reduces the accuracy of the current injection circuitry. Furthermore, it is not always possible to get the desired performance over the whole frequency range because of other limiting factors, such as electrode impedance and nonideal characteristics of the instrumentation. The purpose of an EIS system is to measure the electrical impedance offered by electrodes placed on the biological material and then to interpret the results in terms of an equivalent resistivity or conductivity. In practice, the measured transfer impedance T_Z (the ratio of the measured voltage to the applied current) is a combination of the biological impedance, the electrode/tissue interface impedance and the impedance offered by the instrumentation involved in the measurements.

Generally, a VCCS circuit converts a sine wave voltage V_S into a current I_L whose magnitude is unaffected by load voltage V_L. Figure 2.9 shows a simple model of a monopolar current source, which means that both VCCS and load are grounded.

An analysis of the circuit will show that the voltage V_A at node A is equal to the load voltage V_L and that $I_S = I_Z + I_L$. The load current I_L is given by Eq. (2.6) and is ideally equal to I_S when assuming $Z_S >> Z_L$. In practice, stray capacitances decrease the magnitude of Z_S at higher frequencies. Hence the load current I_L decreases with increasing frequency.

$$I_L = \frac{1}{1 + Z_L/Z_S} \cdot I_S \tag{2.6}$$

The best possible performance from the current source is very important to the design of systems for electrical impedance tomography (EIT), as reported in Denyer et al. (1993, 1994, b), Blad et al. (1994), Li et al. (1994), Lu and Brown (1994) and Jossinet et al. (1994a). These show that it is very difficult to design a VCCS whose

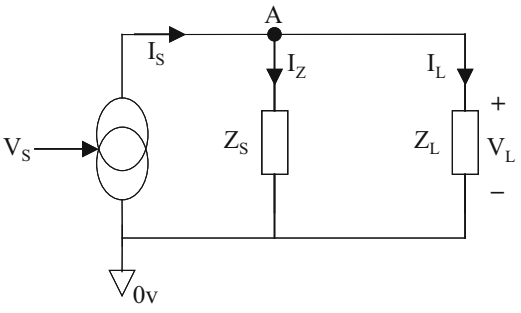

Fig. 2.9 Ideal model of a current source (modified from Webster 1990), where I_S is the output current of the current source controlled by V_S, Z_S is the output impedance of the current source and Z_L is the load

output impedance Z_S is greater than 1 MΩ at frequencies above 1 MHz, as reported in Lu (1995).

The simplest way to implement a VCCS for biological impedance measurements is to use an isolated negative-feedback current source (Smith 1990), where the patient is isolated from the circuitry by a transformer. This current source works well at a single frequency, but it is limited to low frequencies by the performance of the transformer. The majority of VCCS designs for working over a wide frequency range are of two categories: one uses positive feedback in a modified Howland circuit (Cusick et al. 1994; Jossinet et al. 1994b); the other uses current mirror architecture (Casas et al. 1996; Bragós et al. 1994; Riu et al. 1992).

The current mirror design is based on operational amplifier supply currents, as reported in Hart and Barker (1976) and Wilson (1981). Current mirrors for sensing the supply currents of the operational amplifier are used to obtain a VCCS without the use of positive feedback (Toumazou and Lidgey 1989; Denyer et al. 1993). Although high output impedance can be obtained in this type of current source, it was found in practice that there are mismatches between current mirrors which contribute to reduce the frequency response and produce distortions in the current injected into the load. Bragós et al. (1994) have reduced these mismatches by using the integrated current-feedback amplifier AD844 with a DC feedback unit. However, this circuit exhibits large changes in output impedance with consequent changes in load current, as demonstrated by Bertemes-Filho et al. (2000).

The Howland design uses a single operational amplifier with both negative and positive feedback loops, as shown in Fig. 2.10. The output current I_L can be calculated according to Eq. (2.7). It can be seen from Eq. (2.7) that for constant current I_L, it is the ratio R_1/R_2 and R_4/R_3 that is important. Also, the output current I_L will be defined by the resistance R_1 and the input voltage V_i. On the other hand, the output impedance will in theory be infinite if the two feedbacks are identical, i.e. $R_1 = R_2 = R_3 = R_4 = R$. However, mismatching between resistors, stray capacitances and the frequency limits of the op-amp will limit the output impedance.

$$I_L = \frac{V_i}{R_1 + R_L \cdot \left(1 - \frac{R_1}{R_2} \cdot \frac{R_4}{R_3}\right)} \tag{2.7}$$

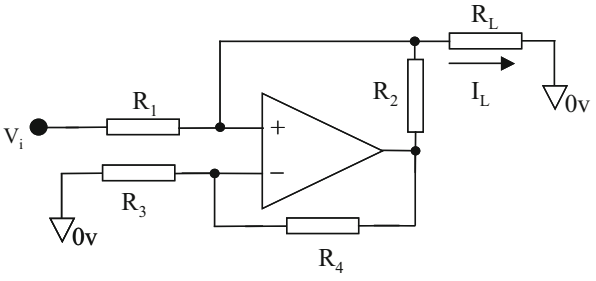

Fig. 2.10 Basic structure of the Howland generator, where V_i is the input voltage and I_L is the driven current in load R_L

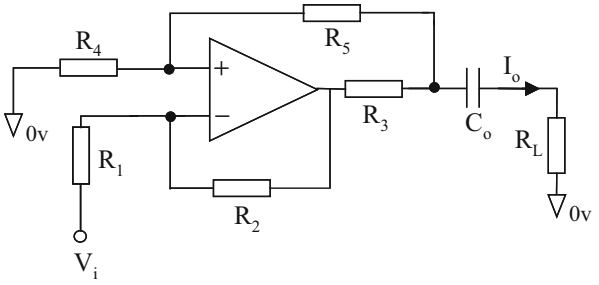

Fig. 2.11 Diagram schematic of the improved Howland current generator, where V_i is the input voltage, I_o is the output current and C_o is the DC-blocking capacitor

In addition to the limitation of the output impedance, the maximum voltage V_L which may develop across the load R_L is limited by the close-loop gain G and by the supply voltages V_{CC} of the operational amplifier, as shown in Eq. (2.8). Higher values of load will saturate the output of the operational amplifier, and then the performance of the VCCS will be affected.

$$V_L = R_L \cdot I_L \leq \frac{V_{CC}}{\mathrm{G}} \tag{2.8}$$

Lu (1995) used an improved Howland generator, which is shown in Fig. 2.11. It can be observed in this circuit that the non-inverting input voltage of the op-amp is a voltage divider of the load voltage. As a result, the fraction of the load voltage acting at this point as a common-mode voltage is decreased. Therefore, the maximum voltage across the load can be increased and thus the current generator's compliance.

It can be derived from Fig. 2.11 that the output current I_o driven into load R_L is given by

$$I_o = \frac{R_4R_2 - R_1 \cdot (R_3 + R_5)}{R_1R_3 \cdot (R_4 + R_5)} \cdot V_L - \frac{R_2}{R_1R_3} \cdot V_i \tag{2.9}$$

where V_L is the voltage across the load.

Equation (2.9) assumes that the operational amplifier is ideal, which means that the output impedance of the op-amp is zero and both input impedance and open-loop gain are infinite. By definition, the output current I_o of a current source should not depend on the load voltage V_L. This is possible by making the value of R_4 equals to the sum of R_3 and R_5 and the values of R_1 and R_2 identical. If these conditions are satisfied, the output current I_o will be determined by R_3, and the output impedance will be infinite. In practice, it is very difficult to keep the output impedance high over the whole frequency range without causing the circuit to oscillate, especially at higher frequencies (e.g. >1 MHz). Many circuit approaches have been used for improving the performance of the enhanced Howland current source (Bertemes-Filho et al. 2013, 2015; Bertemes-Filho and Vincence 2016).

Problems arise when multifrequency systems are required. Careful adjustment of the feedback networks must be done in order to retain stability and to raise

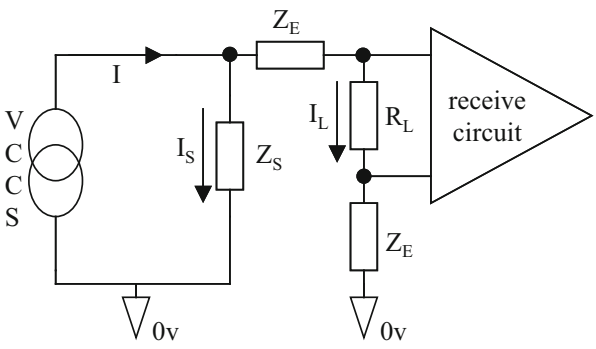

Fig. 2.12 Single-end four-electrode system, where I is the constant driven current, Z_E is the electrode impedance and R_L is the load under study

the output impedance. Some authors have suggested the inclusion of a buffer configured as a voltage follower in the positive feedback loop of the Howland generator (Cusick et al. 1994; Bertemes-Filho et al. 2000). Bertemes-Filho et al. (2000) have concluded that the design of symmetrical current sources should take into account the tolerances of the components used and the output impedance should be calculated under real load condition.

In practice, current generators neither have constant output current nor high output impedance over a wide frequency range. These nonideal characteristics lead to errors in the current injected into the load. The main errors found in a four-electrode system are due to the output impedance Z_S of the current source and the common-mode voltage.

Figure 2.12 shows the effect of the output impedance of a monopolar current source on the load current I_L. It can be seen that the output impedance Z_S of the current source provides a path to some current I_S to flow. Therefore, the accuracy of the load current I_L depends on the output impedance Z_S of the current source, as shown in Eq. (2.10).

$$I_L = \frac{I}{1 + (2Z_E + R_L)/Z_S} \tag{2.10}$$

If the output impedance Z_S of the current source tends to infinity, then the load current I_L will equal that of the current source. Equation (2.10) can be algebraically manipulated in or to show the values of the current source's output impedance Z_S to achieve a load current I_L with an accuracy of at least k%, as shown in Eq. (2.11). Assuming a typical load of 1 kΩ, an electrode impedance of 2 kΩ and an output impedance of 40 kΩ at 1 MHz for the current source (Bertemes-Filho et al. 2000), it can be calculated from Eq. (2.11) that the error in the load current is approximately 11% ($k = 11$) at 1 MHz.

$$Z_S > (2Z_E + R_L) \cdot \frac{100 - k}{k} \tag{2.11}$$

The second source of errors found in drive circuits is related to the common-mode voltage, which appears as an undesired potential across the grounded electrode impedance Z_E and the load R_L (see Fig. 2.12). This potential between the inputs of the receive circuit and ground is usually amplified by a differential amplifier. The common-mode (CM) voltage can have an amplitude much higher than the differential signal across the load to be measured, and hence it must be rejected by the amplifier. Further details about CM voltage are later discussed in this section.

The simplest method of minimising the undesirable CM voltage is by a bipolar current source, which is composed of two-phase opposition controlled current sources (Bertemes-Filho et al. 2009). However, mismatch between the output currents may produce CM voltage at the inputs of the receive circuit. In addition, CM voltage can also be generated by mismatch between drive electrode impedances and by different stray capacitances at each side of the current source.

Also cable capacitances from the receive circuit and the input impedance of the receive circuit produce errors in the driven current and induce common-mode voltages. There are three major approaches to reducing these errors, as described in the following:

1. *Screen driving*: This method consists in driving the cable shield (the second shield for the triaxial cable case) with the signal which is on the cable core by using a buffer configured as a voltage follower, as shown in Fig. 2.13. Then, the cable shield is at the same potential as the signal core itself. In theory, there should then be no current flow through the cable capacitance and hence no attenuation of the signal. Additionally, the first shield of the triaxial cable, which is also known as the outer screen, is earthed to minimise capacitive coupling

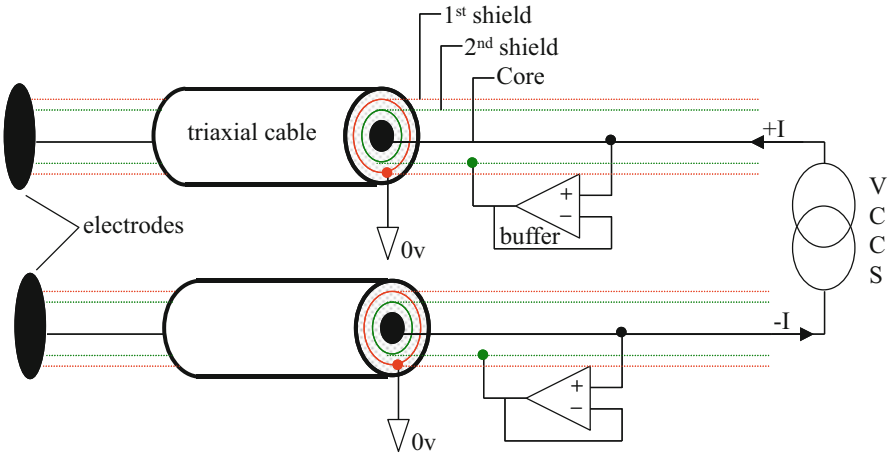

Fig. 2.13 Diagram schematic of the screen driving technique when triaxial cables are used to attach the bipolar current source to the electrodes, where $+I$ is the source current and $-I$ is the sink current

between cables (Lu and Brown 1994). However, the buffer input capacitances to ground cannot be compensated by this technique.

2. *Active electrodes*: The concept is to minimise cable length by placing drive and sense electronics very close to the electrodes. This minimises stray capacitance at the current source output and thus increases the frequency range (Rigaud et al. 1996). Jossinet et al. (1994a, b) connected the output of the current source to the electrode-skin interface. The current sources were encapsulated within the electrode shells. They concluded that the encapsulation removes lead capacitances but the components of the VCCSs should be well matched. Nevertheless, active electrodes need to be small and power has to be supplied to the electronics.
3. *Negative impedance circuit*: It is used to cancel the stray capacitance at the current-source output. This is achieved by producing an equivalent negative impedance in parallel with the stray capacitance. Cook et al. (1994) optimised the output impedance of a current source using a calibration network. Instability due to overcompensation of stray capacitance is the main drawback of this technique. Other attempts using this compensation technique can also be found in Bertemes-Filho et al. (2003, 2004).

In addition to the mentioned approaches, measurement of output current as a method of reducing errors caused by imperfections in the current generator has also been used. However, it is difficult to make the measurements without affecting the circuit performance.

2.4 Basic Voltage Measuring Concepts

The voltage between two electrodes placed on tissue depends mainly on the current which has been injected and the tissue structure. However, electrode construction and position will also affect the measurements. It is desirable that the voltage be measured without interference and noise. The signal needs to be amplified in order to make it compatible with an A/D converter. This chapter will only be concerned with the signal processing prior to A/D converter.

Interference usually means 50 Hz, which is generated by the main power supply, and cross talk such as EMG (ranging between 2 and 500 Hz) and ECG (ranging between 0.05 and 100 Hz). 50 Hz is rejected by the CMRR of the amplifier whereas cross talk by filters. On the other hand, artefacts and noise arise from electrode impedance and the movement of electrodes. The effect of electrode impedance is minimised by tetrapolar measurements. However, noise cannot be totally rejected by a tetrapolar system. The amplified noise may have a higher level than the desired signal. The level of signals to be measured will depend on the distance between the measuring electrodes and on the type of tissue under study, typically ranging between 100 μV and 100 mV.

The majority of the amplifiers used for measuring the potential across tissue have differential inputs and a third input used as the reference potential for the amplifier. The reference is usually the ground of the amplifier and is connected to a third electrode placed on the tissue. The reference to ground causes small differences in the desired signal between the measuring electrodes. The mean of the voltage on the two differential inputs measured with respect to the reference electrode is called the common-mode voltage. It is very important that the differential amplifier rejects common-mode voltage. There are three important characteristics for a good differential amplifier: high input impedance, high CMRR (common-mode rejection ratio) and low noise.

In practice, most biomedical signals are measured by instrumentation amplifiers. The main components of an instrumentation amplifier are two preamplifiers and one amplifier with a differential input and a single-ended output. High input impedance is provided by the two input preamplifiers, and a substantial reduction of the common-mode signal is provided by the output differential amplifier.

Figure 2.14 shows a typical instrumentation amplifier. Resistors R_p set the bias current, which flows into the non-inverting inputs of the operational amplifiers A and B. These resistors define the maximum input impedance of the amplifier, typically greater than 10 MΩ. The preamplifiers A and B offer differential gain but with unity gain to CM signals. The resistors R_f and R_1 determine the differential gain.The inputs V_1 and V_2 are connected to electrodes, which are placed on tissue. Electrodes are characterised by their half-cell potentials, which depend on the electrode properties. For example, gold electrodes present a half-cell potential of 1.68 V. Electrode half-cell potentials limit the gain of the preamplifiers and may lead to saturation. Therefore, the capacitor C_i is introduced to block any DC potential

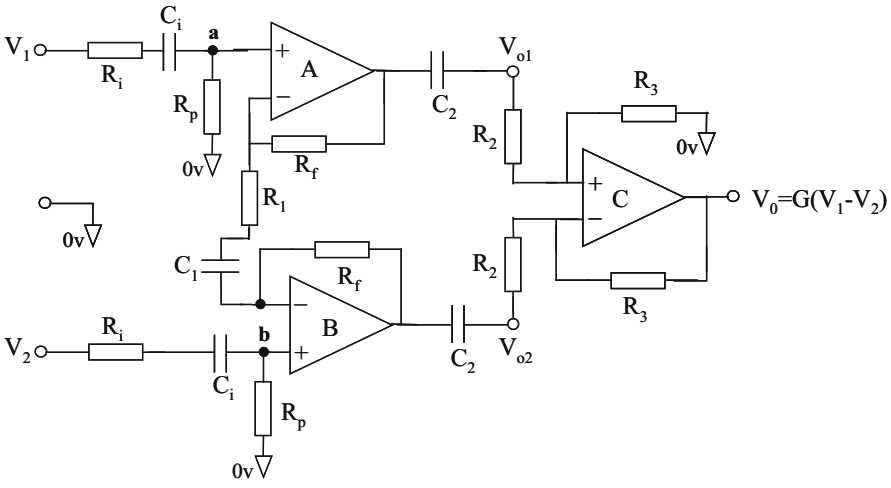

Fig. 2.14 Schematic of an instrumentation amplifier with a differential output, where G is the total differential gain of the instrumentation amplifier

by acting as high-pass filter with the resistor R_p. This capacitor also has a safety function in that it prevents any DC current flow to the electrode in the event of a failure of the preamplifiers A and B. The corner frequency f_0 of the filter is typically 0.05 Hz when $C_i = 33$ nF and $R_p = 100$ MΩ are used, assuming that R_p is much greater than R_i in Eq. (2.12). The AC coupling capacitor C_i does not attenuate the injected sine wave current over the frequency range 1 kHz to 1 MHz covered by this chapter.

$$f_0 = \frac{1}{2\pi \cdot C_i \cdot R_p \sqrt{1 - 2R_i/R_p - \left(R_i/R_p\right)^2}} \tag{2.12}$$

The output voltage V_0 of the differential amplifier shown in Fig. 2.14 can be evaluated according to Eq. (2.13), assuming ideal op-amps.

$$V_0 = \frac{R_p}{R_p + R_i + 1/j\omega C_i} \cdot \left[1 + 2 \cdot \frac{R_f + 1/j\omega C_2}{R_1 + 1/j\omega C_1}\right] \cdot \frac{R_3}{R_2} \cdot (V_1 - V_2) \tag{2.13}$$

Instrumentation amplifiers are not perfect and undesired signals are also amplified. In practice, the output of the instrumentation amplifier shown in Fig. 2.14 consists of the differential input signal (V_1–V_2), an undesired component due to incomplete rejection of common-mode signals and an undesired component due to electrode impedance imbalance. Figure 2.15 shows a model for the receive circuit taking into account both common-mode signal V_{cm} and electrode impedances Z_{e1} and Z_{e2}.

The total output voltage V_0, which is calculated according to Eq. (2.14), can then be evaluated taking into account the CMRR of the amplifier, the electrode impedances and the equivalent input impedance of the amplifier, which is determined by resistor R_p in Fig. 2.14.

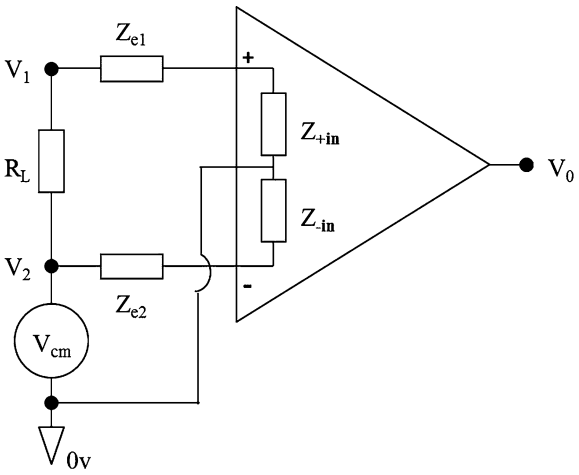

Fig. 2.15 Common-mode signal represented as a voltage generator V_{cm} in the receive circuit, where R_L is the load, Z_{e1} and Z_{e2} are the electrode impedances and $Z_{+\text{in}} = Z_{-\text{in}} = Z_{\text{in}}$ is the equivalent input impedance of the receive circuit

$$V_0 = \mathrm{G} \cdot \left[(V_1 - V_2) + V_{cm} \cdot \left(1 + \frac{1}{\mathrm{CMRR}} - \frac{Z_{in}}{Z_{in} + Z_{e1} - Z_{e2}} \right) \right] \tag{2.14}$$

The equivalent input impedance Z_{in} of an instrumentation amplifier used in EIS systems is typically much greater than the electrode impedance imbalance Z_{e1}–Z_{e2}, and hence the amount of undesired signal at the output of the instrumentation amplifier is mostly dominated by the CMRR. However, stray capacitances connected to ground reduce both the CMRR and the input impedance Z_{in} of the amplifier, especially at frequencies of up to 1 MHz. Reduction of the output voltage V_0 by stray capacitances is not taken into account in Eq. (2.14).

In addition to common-mode voltage and electrode impedance imbalance, noise is also an undesired source of error which appears at the output of the amplifier. Noise can be generated by the amplifier itself. This is usually specified by the manufacturer of the op-amp as an internal voltage noise source e_{n} and internal current noise generator i_{n}. Noise is also generated by movement of the charge carriers, which is represented by an electrical current flowing along a wire of resistance R_{S}. J B Johnson in 1928 showed that the noise power generated in a resistor R_{S} is proportional to the temperature and the value of the resistance; hence it is called *Johnson thermal noise*. The noise components are frequency-dependent. However, the external components of the Howland current source, for example, dominate the total noise leading to an unstable output current and, consequently, resulting in a fully noise voltage across the load under study (Santos and Bertemes-Filho 2017).

Although noise is a big concern in EIS, the use of switches in EIS system gets it even worse, especially at higher frequencies. Usually, multichannel measuring circuits use analogue multiplexers (MUX). MUX has a high effect in the circuitry at higher frequencies due to its input and output capacitances. Furthermore, there are feedthrough stray capacitances due to the use of switches, which link the drive and receive circuits. It is not uncommon to have typical feedthrough capacitances of 10 pF (Lu, 1995). These capacitances degrade the performance of the measurement system, especially at high frequencies. Yet the use of different multiplexers for drive and receive circuits does not eliminate feedthrough and capacitances between cables.

It is common in many receive circuits designed for EIS to use buffers at the receive electrodes as a preamplifier. This increases the input impedance of the receive circuit and reduces the effect of currents through cable and multiplexer stray capacitances. It can also reduce the effect of electrode impedance mismatches. However, the input capacitance of the amplifier degrades the input impedance of the receive circuit, especially at higher frequencies. Nevertheless, using an op-amp with a very low bias current allows R_p (see Fig. 2.14) to be increased. Hence, some researches use op-amps with field-effect transistor (FET) input, whose bias current is about tens of picoamperes. FET op-amps also offer low-noise voltage figures.

Input capacitance can be reduced and hence CMRR improved by using screen driving in the same way as we have described previously in this chapter. Negative impedance converters can also be used for cancelling stray capacitances, which may

be encountered at the input of receive circuits. Cook et al. (1994) used a negative capacitance circuit to obtain high accuracy in a single-frequency and adaptative EIS system. They concluded that the circuit must be constantly trimmed in order to achieve accurate measurements.

2.5 Desired Hardware Specifications

For a giving sine wave input voltage, the output current magnitude of the monopolar VCCS should be constant with respect to the frequency range 1 kHz to 1 MHz with a maximum deviation of 1% from the nominal value. The magnitude of the output current should also remain constant with respect to the load ranging between 50 Ω and 5 kΩ. In the case of a bipolar current source, both current source and sink should be balanced with a maximum difference of 0.1% between the nominal values.

It is also important that the output impedance of both monopolar and bipolar current source be much greater than the total load between the injecting electrodes. The total load is approximately the resistance of the material under study summed with the impedance of both electrodes. The output impedance should be at least 100 times greater than the total load at the highest frequency, i.e. 1 MHz.

The gain of the receive circuit must be able to handle input voltage ranging between 1 $mV_{p\text{-}p}$ and 80 $mV_{p\text{-}p}$, when 1 $mA_{p\text{-}p}$ current is applied to the biological material under study. The input impedance is specified to be higher than 100 kΩ within the frequency range 1 kHz to 1 MHz.

The common-mode signals should be kept as low as possible by obtaining a CMRR greater than 80 dB over the frequency range, which means to have CM voltages smaller than 10 $\mu V_{p\text{-}p}$ with respect to the smallest measured signal of 1 $mV_{p\text{-}p}$. The instrumentation amplifier is implemented for obtaining a gain of 100. The noise voltage must be at maximum 1% of the measured biological signal. The total normalised gain must be flat within the specified frequency range, for example, as shown in Fig. 2.16.

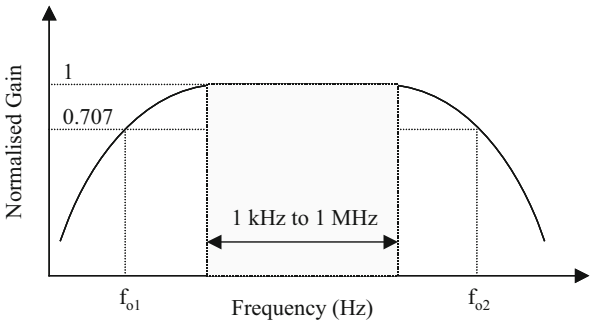

Fig. 2.16 Bode plot of the theoretical gain for the receive circuit, where f_{o1} and f_{o2} are the low and high corner frequencies, respectively

2.6 Discussions

The majority of VCCSs in EIS systems are designed to work over a wide frequency range and to have high output impedance. Both Howland and current mirror-type circuits can achieve an adequate performance. However, the components have to be very well matched in both of circuits. Output impedance greater than 100 kΩ at 1 MHz is very difficult to achieve, unless an additional compensating circuit is used.

A wide bandwidth Howland current generator may suffer from instability problems, unless very accurate components are used and care is taken with circuit layout. Instability seems not to be a problem in current mirror circuits although layout will still be important to minimise stray capacitances. However, the accuracy of the output current depends on the accuracy of the current copied by the transistors.

Nevertheless, stray capacitances degrade the output impedance of all VCCSs and also the voltage measurement circuits. Undesired stray capacitances can be significantly reduced by a negative impedance converter. However, instability can be a problem in multichannel EIS systems.

Although an accurate constant current can be driven into the tissue under study, the measured voltage will always contain undesired components which cannot be completely rejected. Most voltage measuring circuits are based on the three-op-amp configuration as an instrumentation amplifier. High input impedance is required for accurate measurements. However, mismatch of feedback resistors in the differential amplifier stage degrades the CMRR of the amplifier and hence the input impedance.

Common-mode voltage generated by mismatching between electrode impedances is the main source of error in this type of measuring system. Mismatches of this kind are encountered at the electrode-electrolyte interface. Cable stray capacitances also introduce errors in the voltage measurements.

There is a significant reduction of cable stray capacitances when part of the drive and receive circuits are built very close to electrodes. This technique increases significantly the output impedance of the drive system, and hence improvement in the CMRR can be achieved.

Although accurate measurements can be achieved, the performance of the VCCS and the instrumentation amplifier is not well controlled due to the unknown tissue impedance and to stray capacitances which might be encountered in the input circuitry. Therefore, calibration is very important when tissue characterisation is required. The overall gain of the system needs to be measured when the probe is applied to saline solutions of known conductivities. These solutions must be chosen to have similar conductivities to the tissue of interest.

References

Bertemes-Filho, P. (2002). *Characterisation using an impedance spectroscopy probe*. Ph.D. Thesis, Sheffield, England.

Bertemes-Filho, P., Brown, B. H., & Wilson, A. J. (2000). A comparison of a modified Howland circuits as current generators with current mirror type circuits. *Physiological Measurement, 21*(Suppl. 1A), 1–6.

Bertemes-Filho, P., Felipe, A., & Vincence, V. C. (2013). High accurate Howland current source: Output constraints analysis article. *Circuits and Systems, 4*(7), 451–458.

Bertemes-Filho, P., Lima, R. G., Amato, M. B. P., & Tanaka, H. (2004). Capacitive-compensated current source used in electrical impedance tomography. In *International conference on electrical bio-impedance*, Gdansk, Poland, 20–24 June 2004.

Bertemes-Filho, P., Lima, R. G., & Tanaka, H. (2003). An adaptive current source using a negative impedance converter (NIC) for electrical impedance tomography (EIT). In *International Congress of Mechanical Engineering*, June, Sao Paulo, Brazil.

Bertemes-Filho, P., Negri, L. H., & Vincence, V. C. (2015). Designing a mirrored Howland circuit with a particle swarm optimisation algorithm. *International Journal of Electronics, 1*, 1029–1037.

Bertemes-Filho, P., Paterno, A.S., & Pereira, R. M. (2009). Multichannel bipolar current source used in electrical impedance spectroscopy: Preliminary results. In O. Dössel, & W. C. Schlegel (Eds.), *World Congress on Medical Physics and Biomedical engineering*, September 7–12, 2009, Munich, Germany. IFMBE proceedings, Vol 25/7. Berlin, Heidelberg: Springer.

Bertemes-Filho, P., & Vincence, V. C. (2016). Howland current source for wideband bioimpedance application. In *XVI International Conference on Electrical Bioimpedance*, June.

Blad, B., Lindstrom, K., Bertenstam, L., Person, B. R. R., & Holmer, N. G. (1994). A current injecting device for electrical impedance tomography. *Physiological Measurement, 15*(Suppl. 2A), 69–77.

Bragós, R., Rosell, J., & Riu, P. J. (1994). A wide-band AC-coupled current source for electrical impedance tomography. *Physiological Measurement, 15*(Suppl. 2A), 91–99.

Brown, B. H., Smallwood, R. H., Barber, D. C., Lawford, P. V., & Hose, D. R. (1999). *Medical physics and biomedical engineering*. Bristol: Institute of Physics Publishing.

Casas, O., Rosell, J., Bragós, R., Lozano, A., & Riu, P. J. (1996). A parallel broadband real-time system for electrical impedance tomography. *Physiological Measurement, 17*(Suppl. 4A), 1–6.

Cole, K. S., & Cole, R. H. (1941). Dispersion and absorption in dielectrics. *The Journal of Chemical Physics, 9*, 341–351.

Cook, R. D., Saulnier, G. J., Gisser, D. G., Goble, J. C., Newell, J. C., & Isaacson, D. (1994). ACT3: A high-speed, high-precision electrical impedance tomograph. *IEEE Transactions on Biomedical Engineering, 41*(8), 713–721.

Cusick, G., Holder, D. S., Birquett, A., & Boone, K. (1994). A system for impedance imaging epilepsy in ambulatory human subjects. *Innovation et technologie en biologie et médecine, 15*, 33–39.

Denyer, C. W., Lidgey, F. J., McLeod, C. N., & Zhu, Q. S. (1994). Current source calibration simplifies high-accuracy current source measurement. *Innovation et technologie en biologie et médecine, 15*(Spécial 1), 47–55.

Denyer, C. W., Lidgey, F. J., Zhu, Q. S., & McLeod, C. N. (1993). High output impedance voltage controlled current source for bio-impedance instrumentation. *Proceedings of the 15th annual international conference of the IEEE engineering in medicine and biology society, San Diego*, *15*(2), 1026–1027.

Denyer, C. W., Lidgey, F. J., Zhu, Q. S., & McLeod, C. N. (1994). A high output impedance current source. *Physiological Measurement, 15*(Suppl. 2A), 79–82.

Foster, R. F., & Schwan, H. P. (1989). Dielectric properties of tissues and biological materials: A critical review. *Critical Reviews in Biomedical Engineering, 17*(1), 25–104.

González-Correa, C. A., Brown, B. H., Smallwood, R. H., Kalia, N., Stoddard, C. J., Stephenson, T. J., et al. (1999). Virtual biopsies in Barrett's esophagus using an impedance probe. *Annals of the New York Academy of Sciences, 873*, 313–321.

Griffiths, H., & Ahmed, A. (1987). A dual-frequency applied potential tomography technique: Computer simulations. *Clinical Physics and Physiological Measurement, 8*(Suppl. A), 103–107.

Hart, B. L., & Barker, R. W. (1976). D.C. matching errors in the wilson current source. *Electronics Letters, 12*(15), 389–390.

Hollas, J. M. (1998). *High resolution spectroscopy*. Chichester: John Willey & Sons.

Jossinet, J., Tourtel, G., & Jarry, R. (1994a). Performance and operation of a set of wideband current generators for EIT. *Innovation et technologie en biologie et médecine, 15*, 40–46.

Jossinet, J., Tourtel, C., & Jarry, R. (1994b). Active current electrode for in vivo electrical impedance tomography. *Physiological Measurement, 15*(Suppl. 2A), 83–90.

Land, R., Cahill, B. P., Parve, T., Annus, P., & Min, M. (2011). Improvements in design of spectra of multisine and binary excitation signals for multi-frequency bioimpedance measurement. *Conference proceedings of the IEEE engineering in medicine and biology society,* Boston, MA, USA.

Li, J., Joppek, C., & Faust, U. (1994). An isolated wideband current source used in multifrequency electrical impedance tomography. *Innovation et technologie en biologie et médecine, 15*, 63–68.

Lozano, A., Rosell, J., & Pallás-Areny, R. (1990). Two-frequency impedance plephysmography real and imaginary parts. *Medical & Biological Engineering & Computing, 28*, 38–42.

Lu, L. (1995). *Aspects of an electrical impedance tomography spectroscopy (EITS) system*. Ph.D. Thesis, Sheffield: University of Sheffield, UK.

Lu, L., & Brown, B. H. (1994). The electronic and electronic interface in an EIT spectroscopy system. *Innovation et technologie en biologie et médecine, 15*(1), 97–103.

McAdams, E. T. (1987). *A study of Electrode-Tissue Impedance Encountered in Cardiac Pacing*. Thesis, lEEDS: University of Leeds, UK.

Min, M, Pliquett, U., Nacke, T., Barthel, A., Annus, P., & Land, R. (2007). Signals in bioimpedance measurement: Different waveforms for different tasks. In H. Scharfetter & R. Merwa (Eds.), *13th International Conference on Electrical Bioimpedance and 8th Conference on Electrical Impedance Tomography*, Graz, Austria.

Nahvi, M., & Hoyle, B. S. (2009). Electrical impedance spectroscopy sensing for industrial processes. *IEEE Sensors Journal, 9*(12), 1808–1816.

Paavle, T., Min, M., & Parve, T. (2012). Aspects of using chirp excitation for estimation of bioimpedance spectrum. In S. Salih (Ed.), *Fourier transform—Signal processing* (pp. 237–256). Rijeka: InTech.

Paterno, A. S., Negri, L. H., & Bertemes-Filho, P. (2012). Efficient computational techniques in bioimpedance spectroscopy. In G. R. Naik (Ed.), *Applied biological engineering—Principles and practice*. Rijeka: InTech. https://doi.org/10.5772/36307

Pethig, R. (1984). Dielectric properties of biological materials: Biophysical and medical applications. *IEEE Transactions on Electrical Insulation, 19*, 453–474.

Pethig, R. (1987). Dielectric properties of body tissues. *Clinical Physics and Physiological Measurement, 8*(Suppl. A), 5–12.

Pliquett, U., Frense, D., Schönfeldt, M., Frätzer, C., Zhang, Y., Cahill, B., et al. (2010). Testing miniaturized electrodes for impedance measurements within the E-dispersion—A practical approach. *Journal of Electrical Bioimpedance, 1*, 41–55.

Raghed, A. O., Geddes, L. A., Bourland, J. D., & Tacker, W. A. (1992). Tetrapolar electrode system for measuring physiological events by impedance. *Medical & Biological Engineering & Computing, 30*, 115–117.

Record, P., Gadd, R., & Vinther, F. (1992). Multifrequency electrical impedance tomography. *Clinical Physics and Physiological Measurement, 13*(Suppl. 2A), 67–72.

Riu, P. J., Rosell, J., Lozano, A., & Pallás-Areny, R. (1992). A broadband system for multifrequency static imaging in electrical impedance tomography. *Clinical Physics and Physiological Measurement, 13*(Suppl A), 61–65.

Rigaud, B., & Morucci, J. P. (1996). Bioelectrical impedance techniques in medicine. Part III: Impedance imaging, first section: General concepts and hardware. *Critical Reviews in Biomedical Engineering, 24*(4–6), 467–597.

Santos, S. F., & Bertemes-Filho, P. (2017). Note: Temperature effects in the modified Howland current source for electrical bioimpedance spectroscopy. *Review of Scientific Instruments, 88*(7), 076103.

Smith, R. W. M. (1990). *Design of a real-time impedance imaging system for medical applications*. Ph.D. Thesis, Sheffield: University of Sheffield, UK.

Toumazou, C., & Lidgey, F. J. (1989). Novel current-mode instrumentation amplifier. *Electronics Letters, 25*, 228–230.

Waterworth, A., Brown, B. H., Smallwood, R., & Milnes, P. (2000). Cole equation modelling to measurements made using an impulse driven transfer impedance system. *Physiological Measurement, 21*, 137–144.

Webster, J. G. (1990). *Electrical impedance tomography*. Bristol: Adam Hilger Press.

Wilson, B. (1981). A low-distortion bipolar feedback current amplifier technique. *Proceedings of the IEEE, 69*(11), 1514–1515.

Yang, Y., Kang, M., Lu, Y., Wang, J., Yue, J., & Gao, Z. (2010). Design of a wideband excitation source for fast bioimpedance spectroscopy. *Measurement Science and Technology, 22*, 013001.